



TECHNICAL ARTICLE

Investigation Microstructure and Mechanical Properties of Ramor and Stainless Steel Joined by Friction Welding

Edip ÇETKİN, Anıl İMAK, and İhsan KİRİK

Submitted: 3 July 2022 / Revised: 26 October 2022 / Accepted: 30 October 2022 / Published online: 17 November 2022

In this study, Ramor 500 and AISI 316 austenitic stainless steels with different properties were welded by friction welding using different two rotation speeds and three different friction times. The friction welding processing was carried out rotation speed at 1800 and 2200 rpm and friction times of 3, 5, and 7 s. SEM, EDS, microhardness, and tensile tests were performed, respectively, to determine the effects of processing parameters such as rotation speed and friction time on microstructure and mechanical properties. In the tensile tests, the ultimate stress was obtained as 585.6 MPa in the welds made at 2200 rpm and 3 s (S1) parameters. In EDS analysis, the excess of Cr element on the metal side of AISI 316 and the excess of Fe ratio in Ramor 500 metal were determined. In the experimental results, it was determined that the microstructure and mechanical properties were significantly affected by the welding parameters varying within the selected conditions range. The tensile strength of the welded joints made at the maximum rotation speed and minimum friction times was higher.

Keywords AISI 316, friction welding, mechanical properties, microstructure, Ramor 500

1. Introduction

A armor-grade steels possessing high strength and hardness are widely used in the production of military armored vehicles and its equipment (Ref 1-3). Armor-grade steels are prone to cold cracking due to their high carbon content (Ref 4), so they are complex to weld. For this reason, joining armor steels with welding methods requires careful control of welding procedures to prevent hardness losses in the heat-affected zones (HAZ) (Ref 5-7). Cracks appear in the fusion line (FL) between weld metal, HAZ, and base metal as a result of higher carbon content and hardness. These cracks cause damage in the use of military equipment and vehicles over time. Considering that especially armor steels are used in ballistic applications, it is important to meticulously choose the welding methods used in joining armor steels.

Austenitic stainless steels, which have high in chromium, are commonly used in a wide range of industries due to their superior mechanical properties and excellent corrosion resistance such as energy systems, chemical containers, marine tools, home appliances, and food industries (Ref 8-10). Austenitic stainless steels, particularly AISI 316 stainless alloy, are currently the most common (Ref 11). Because of their low

nickel content, austenitic stainless steels have good weldability. However, the melting and solidification processes used in fusion welding can destroy the advantageous duplex microstructure of these stainless steels. As a result, during the fusion welding process, harmful intermetallic phases can form in the microstructure. Other factors such as higher ferrite content and coarser grains can reduce fusion-welded joints' corrosion resistance and mechanical properties (Ref 12-18).

TIG, MIG, MAG and Electrode arc (based on melting) are traditional welding methods to be used to join similar metals perfectly. However, there are some problems when joining two metals with different chemical and physical properties. These are the problems caused by residual stresses, slags, pores, high heat inputs and the formation of fragile intermetallic phases (Ref 19, 20). Scientific studies and efforts are being made to reduce these problems caused by traditional welding methods, which is a joining technique based on melting. One of the studies focused on the friction welding technique, a method of solid-state welding. Friction welding is a relatively new method and is commercially available. In this method, the inconveniences caused by fusion welding methods are avoided since the materials are friction welded before they reach the melting temperature.

Similar and different metal joints are employed in a broad range of applications due to many advantages of solid-state welding methods, such as FSW (Ref 21-26), friction welding (Ref 27-39), and ultrasonic welding (Ref 40). For welded joints of armor steels, Unfried et al. studied the microstructure of arc-welded armor plate steel (MIL A46100) experimentally and numerically. To that end, they presented a modeling approach to assess the solid-state microstructure development of steels after arc welding. The proposed algorithm was adequate for quantitatively describing both major properties and minor details of the microstructure of a welded MIL A46100 armor steel plate. The reliability of each task, however, was not assessed (Ref 41). Furkan et al. investigated the microstructure and mechanical properties of armor 500/AISI 2205 steel joints

Edip ÇETKİN, Department of Electricity and Energy, Batman University, Batman, Turkey; Anıl İMAK, Department of Mechanical Engineering, Bingöl University, Bingöl, Turkey; and İhsan KİRİK, Department of Machinery and Metal Technologies, Bingöl University, Bingöl, Turkey. Contact e-mails: edip.cetkin@batman.edu.tr, aimak@bingol.edu.tr, and ikirik@bingol.edu.tr.

welded by friction welding at different welding parameters. Microstructural analysis was performed using SEM and the mechanical test was done using tensile tests. They indicated that the welding parameters had a significant effect on the microstructural and mechanical examinations. The maximum tensile stress (1020 MPa) was obtained in friction time of 8 s and under friction pressure of 80 MPa (Ref 42). Taskaya et al. examined the joining of Ramor 500 steel by submerged arc welding and its thermal analysis in the ANSYS software. They indicated that 250 A had a full density in all joints in terms of the density of the welded joints. Furthermore, they stressed that both the findings of the experimental studies and the results of the finite element solutions were compatible with each other (Ref 43). Ipek and Elaldi welded armor steels through gas metal arc welding by cutting different weld grooves and geometries. Tensile, compression and bending tests were run to determine the effects of joints welded in different welds, grooves, and geometries. The best tensile results were achieved from the weld joint employing a welding angle of 54 degrees and V-welding groove geometry as a result of the experiments. Furthermore, they stated that the best compression strength was obtained in a welding groove angle of 48 degrees and the x-welding groove geometry parameter (Ref 44). Savic and Cabrilo joined Protac 500 armor steel with opened V-welding groove using gas metal arc welding at heat inputs of 1.29 and 1.55 kJ/mm. Izod, Charpy and ballistic tests were run for the joints. They stated that there were protrusions in the HAZs of the welding with a heat input of 1.55 kJ/mm in the ballistic tests. The highest energy absorption was achieved in the experiments at 20 °C ambient temperature during the Izod Charpy tests that were run at 20, 0, -20 and -40 °C. They also noted that the fractures in the SEM images occurred in the form of a ductile-brittle mechanism. They underlined that the sample was broken at the lowest energy absorption in the test at -40 °C (Ref 45). Magudeeswaran et al. investigated the metallurgical properties of welded armor steel joints utilized in the manufacturing of a combat vehicle. They utilized austenitic stainless steel (ASS), high nickel steel (HNS), and low hydrogen ferritic (LHF) steel consumables for that purpose. They preferred shielded metal arc welding (SMAW) and flux-cored arc welding (FCAW) methods for welded joints. They stated that the joints welded by utilizing LHF consumables exhibited a lower degree of HAZ softening, and also, no hydrogen-induced cracking was observed in joints manufactured using LHF consumables (Ref 46).

When looking at the studies in the literature, it is possible to see that countless studies join the same or different materials. However, studies on joining different properties of Ramor and stainless steels with friction welding are scarcely any. For this purpose, the use of friction welding for joining dissimilar materials, such as Ramor and stainless steels, is increasingly meeting expectations to a large extent. In particular, the joining process of dissimilar metal pairs such as Ramor and stainless steel is needed in the defense industry. From this point of view,

in this study, the joinability of Ramor and stainless steels with different properties was examined, and this gap was tried to be eliminated by determining the microstructure and mechanical properties.

2. Experimental Detail

Commercially available Ramor 500 and AISI 316 steels were employed in this study. Ramor 500 steel, supplied in plates with sizes of 300 × 100 × 12 mm (length, width, and thickness), was first cut into 100 × 12 × 12 mm for friction welding. It was then machined on the CNC machine to have a diameter of 12 mm and a length of 120 mm. AISI steel was supplied in a length of 100 mm and a diameter of 12 mm. Table 1 shows the chemical composition of Ramor 500 and AISI 316 steel, and Table 2 shows its mechanical properties.

2.1 Welding Processes

In order to obtain a quality weld from the samples to be joined in the friction welding process, the surfaces to be rubbed with each other must first be smooth and flat. In other words, when the samples are in contact with each other on the same axis, the surfaces must fit perfectly. After the samples to be welded for this process were prepared with a diameter of 12 mm and a length of 100 mm, the contact surfaces of the samples were processed on the CNC machine and made flat. Afterward, after the samples were fixed to the opposite mirrors in the welding machine (Fig. 1), the surfaces to be rubbed (the surfaces to be welded) were checked again. After all the samples were prepared, the welding process was made. The welds were made using the parameters (Table 3) based on the literature studies, in a PLC controlled continuously driven welding machine.

Following the sample preparation steps, Ramor 500 and AISI 316 steels were joined by friction welding using Ramor 500 and AISI 316 steels were successfully joined by friction welding using the parameters given in Table 3. Figure 1 shows the friction welding machine and its image taken during a welding process. In the welding process, at least three samples from each parameter were welded.

2.2 Mechanical and Microstructure Samples

Following the completion of friction welding of Ramor 500 and AISI 316 steels, samples for experimental studies were prepared. For tensile tests, all samples were machined on a CNC machine according to ASTM E8 standard. Figure 2 shows 3D drawings of tensile specimens prepared from welded specimens according to ASTM E8 standard. After completing the sample preparation for the tensile tests, they were tested on the SHMADZU tensile testing device. The experiments were carried out at a feed rate of 1 mm/min and an ambient

Table 1 Chemical compositions of Ramor 500 and AISI 316 steels (%wt.) (Ref 43, 47)

Material	C	Mn	Si	P	S	Cr	Mo	Ni	N	B	Fe
AISI 316 [47]	≤ 0.03	≤ 0.2	0.1	≤ 0.045	≤ 0.015	16.50-18.50	2.0-2.5	10 – 13	≤ 0.110	...	Balance
Ramor 500 [43]	0.32	1.50	0.70	0.015	0.005	1.00	0.70	2.00	...	0.005	Balance

temperature of 25 °C. All experiments were repeated three times. The force–elongation graphs were then created by taking the average of these three tests.

SEM images were captured to examine the microstructures in the weld zone. For this purpose, the samples were cut in 30 × 30 mm dimensions perpendicular to the joint surface, and their surfaces were polished with 3 μm diamond paste after being ground with 80-1200 mesh sandpaper to observe the structural change in the joint area of the samples. For the hardness test, the samples were cut in 30 × 30 mm dimensions perpendicular to the cross section of the weld and they were measured in Vickers (HV) units at 1 mm intervals under a load of 20 g.

3. Results and Discussion

As has been already explained, mechanical tests and microstructure analysis were performed, and their corresponding testing samples were welded by friction welding. These samples were jointed with different friction pressure and friction times. The most important part of mechanical testing

was ultimate tensile strength tests, but the SEM analysis and microhardness tests were performed, too.

3.1 Macro- and Microstructure Analyses of Welding Samples

Figure 3 shows post-welding and post-tensile test macrostructure images of Ramor 500/AISI 316 material pairs that were friction welded at 1800 and 2200 rpm rotation speeds and for friction times of 3, 5, and 7 s.

When the post-welding samples, shown in Fig. 3(a), were evaluated with the naked eye, no cracks, voids, or broken structures were noticed in the samples joined with different welding parameters. The flash sizes differed based on the Ramor 500/AISI 316 material pair utilized in welded joints and their mechanical properties. Under constant rotational speed conditions, the flash size increased depending on the friction time. Furthermore, the flash size was larger on the AISI 316 steel side than on the Ramor 500 steel side. This can be associated with the lower thermal conductivity of stainless steel than Ramor steel. Following the tensile tests shown in Fig. 3(b), fractures occurred in the AISI 316 material at the

Table 2 Mechanical properties of 316 austenitic stainless steel and Ramor 500 steel

Materials	Tensile strength, MPa	Elongation, %	Microhardness, HV 0.5
AISI 316	615.361	42.36	182
Ramor 500	1700	14	517-603

Table 3 Parameters used in the welding process

Sample no	Rotation speeds, rpm	Friction Pressure, MPa	Friction times, s
S1	2200	50	3
S2	2200	50	5
S3	2200	50	7
S4	1800	50	3
S5	1800	50	5
S6	1800	50	7

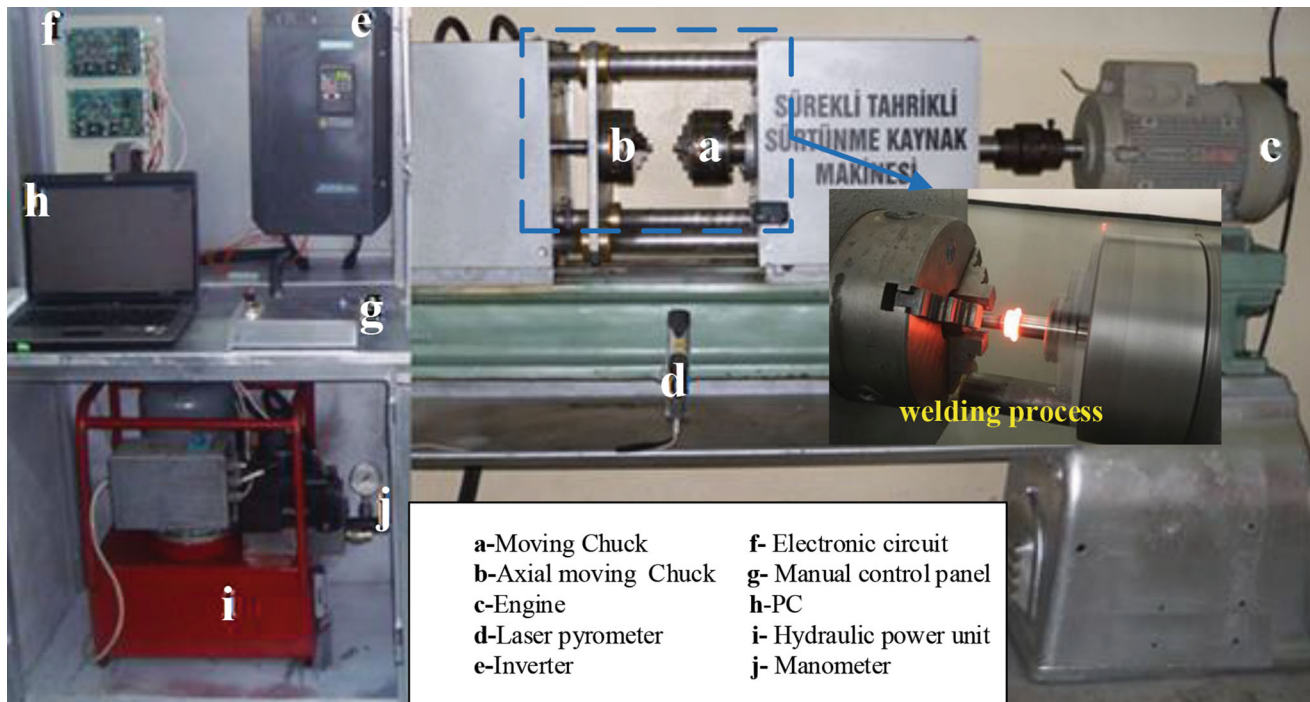


Fig. 1 Continuous drive friction welding machine with which welds were made

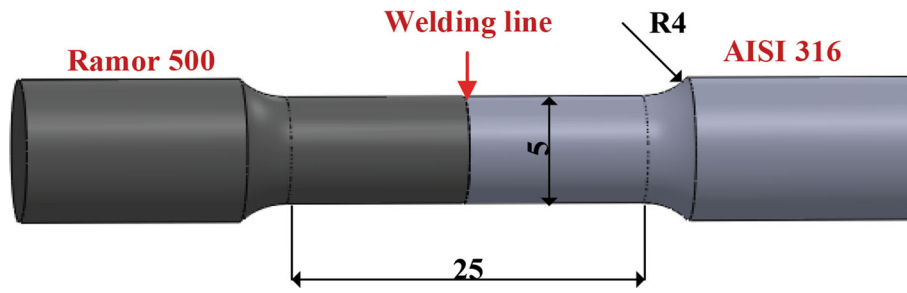


Fig. 2 3D drawings of welded specimens (all units mm)

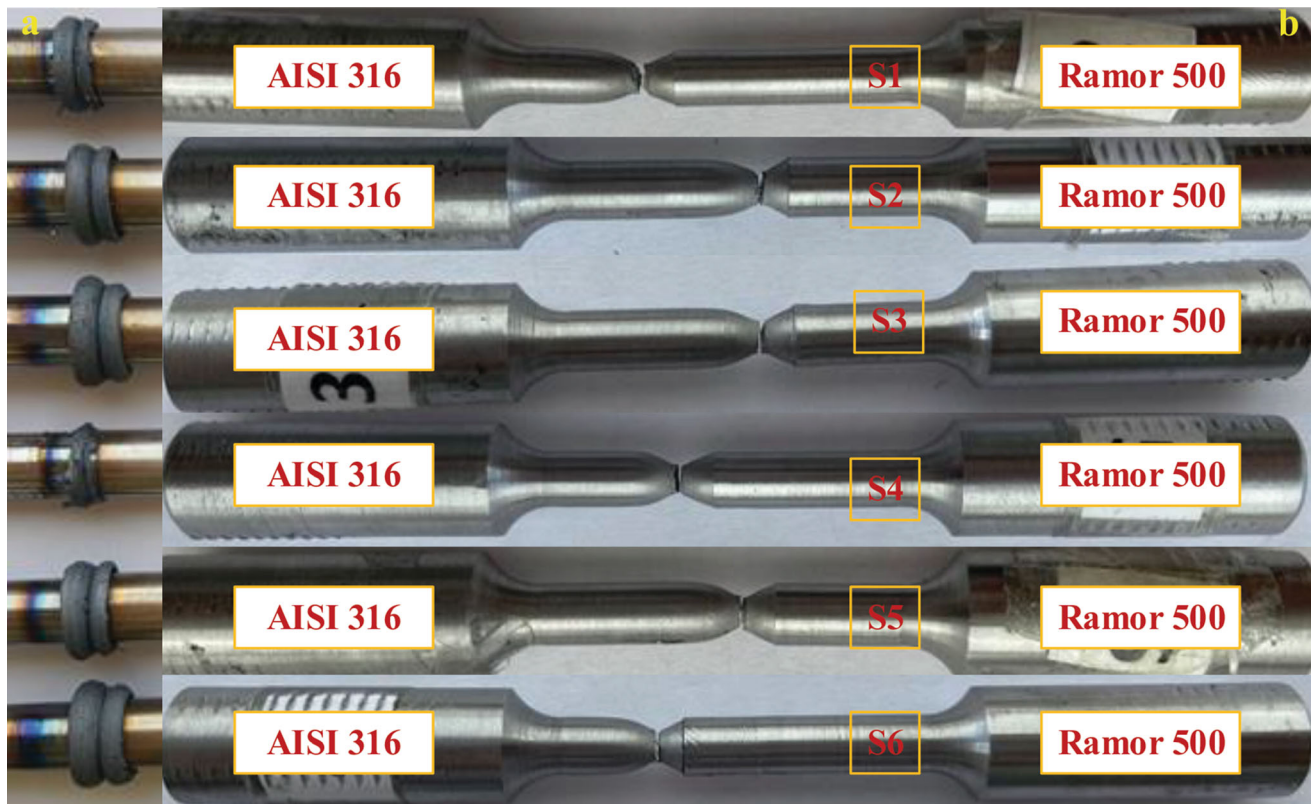


Fig. 3 Macro-displays structure (a: after welding, b = after tensile)

joints welded at 1800 and 2200 rpm for 3 s (S1 and S2) of the Ramor 500/AISI 316 material pairs in the macrostructures of the welded samples. Furthermore, ductile form fractures occurred by elongating on the AISI 316 side. The fractures occurred in the HAZ in the joints welded for 5 and 7 s. This is thought to be due to the fact that the weld zone had more heat input in the joints welded for 5 and 7 s than the joints welded for 3 s. Following the tensile tests, microstructure images were captured to further analyze the fracture zones of the fracture samples.

Figure 4 and 5 shows SEM images of the samples S1 and S6. SEM images were captured to analyze the metallurgical conditions in the cross section of Ramor 500/AISI 316 material pairs welded through friction welding at different welding parameters. As indicated in the studies of Seregin and Sabatsev (Ref 48) and Kirik et al. (Ref 49), the joint was separated into deformation zone (DZ), fully plasticized deformed zone (FPDZ) and the base metal (BM) in microstructure analyses. Microstructure examinations revealed gaps in the welding intermediary transition zones and the Ramor 500/AISI 316 base

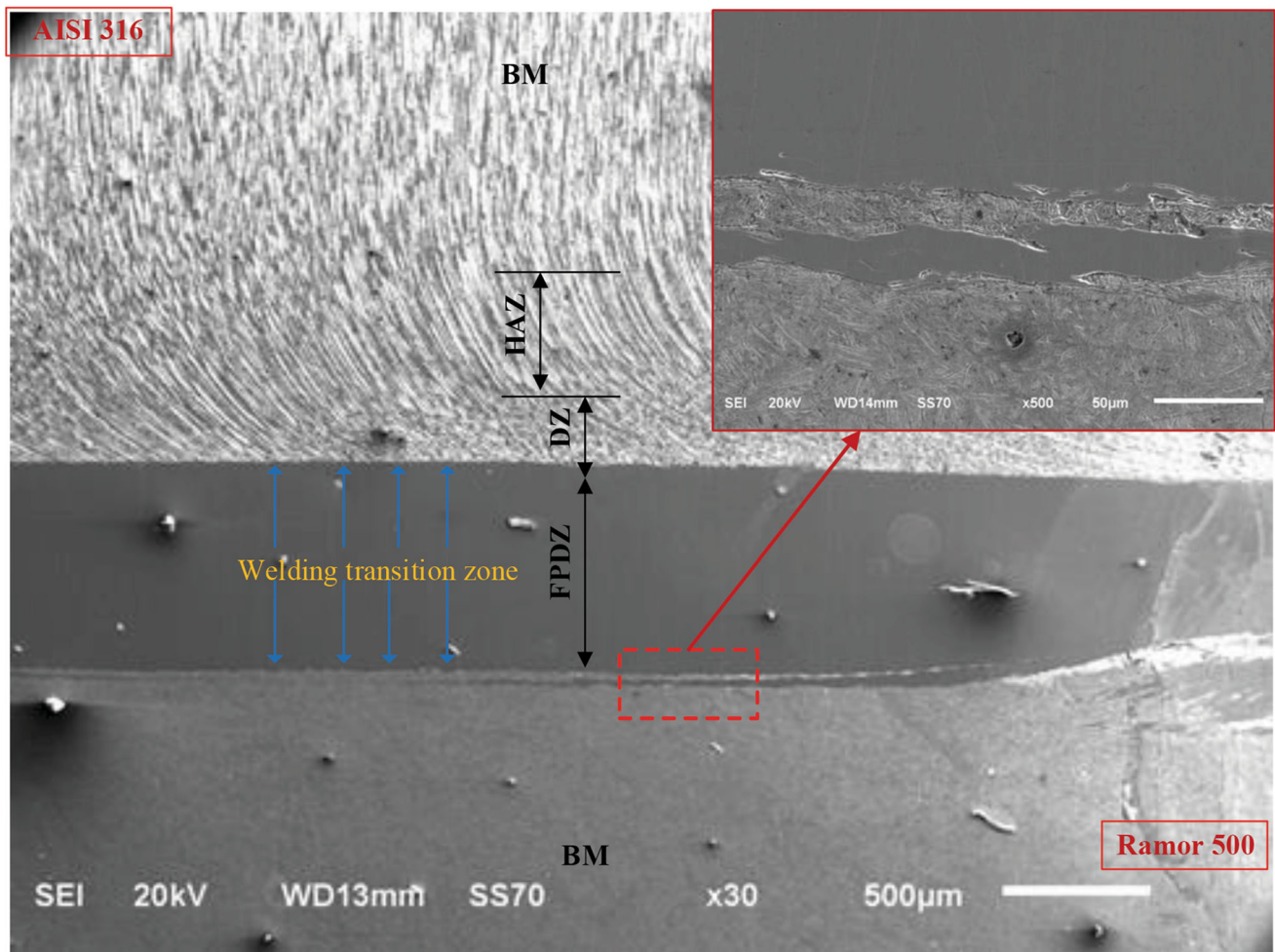


Fig. 4 SEM image of the weld cross section of sample S1

metal pairs of the sample S6, resulting in the failure of a full joint. This condition appeared more clearly on the AISI 316 side. This is thought to be due to the fact that the welding parameters of 1800 rpm and 7 s selected for the sample S6 failed to fully plasticize both materials. When examining the weld metal, partial fine-grained structures were observed to form near the Ramor 500 side, but coarser grains appeared near the AISI 316 steel side. This was caused by the fact that the plasticization temperatures and thermal conductivity coefficients of Ramor 500 and AISI 316 material pairs were different. The SEM images of the weld intermediary cross section of the sample S1 showed more smooth joints between the weld transition zones and the base metals. The gaps that formed in the sample S6 were not observed there. This condition is thought to make both Ramor 500 and AISI 316 material pairs more viscous with the selected welding parameters, and therefore, smooth joints were provided in the deformation zone and welding intermediary cross sections. Furthermore, the

distance between the weld metal and the HAZ was substantially less. The HAZ, on the other hand, may be seen more clearly in the sample S1. The studies have also indicated that parameters, such as friction time and rotation speed, are important elements in joining the material pairs to be joined at the appropriate viscous temperature (Ref 50-54).

When Ramor steels are joined by other steels with fusion welding methods, such as TIG, MIG, PTA, FSW, Laser and Submerged Welding (Ref 43, 55-58), the molten weld pool not only causes negative changes in the microstructure, but also causes the loss of armor properties of the steel in the weld zone and HAZ. In order to eliminate these negativities, friction welding, whose joining temperature is below the melting temperatures of the joined parts and whose joining time is very short, has provided a great advantage (Ref 42). The welding zone of the parts joined by friction welding was effective in a narrow region. It is clear that the joining of Ramor steel and Stainless steels with friction welding does not affect the Ramor

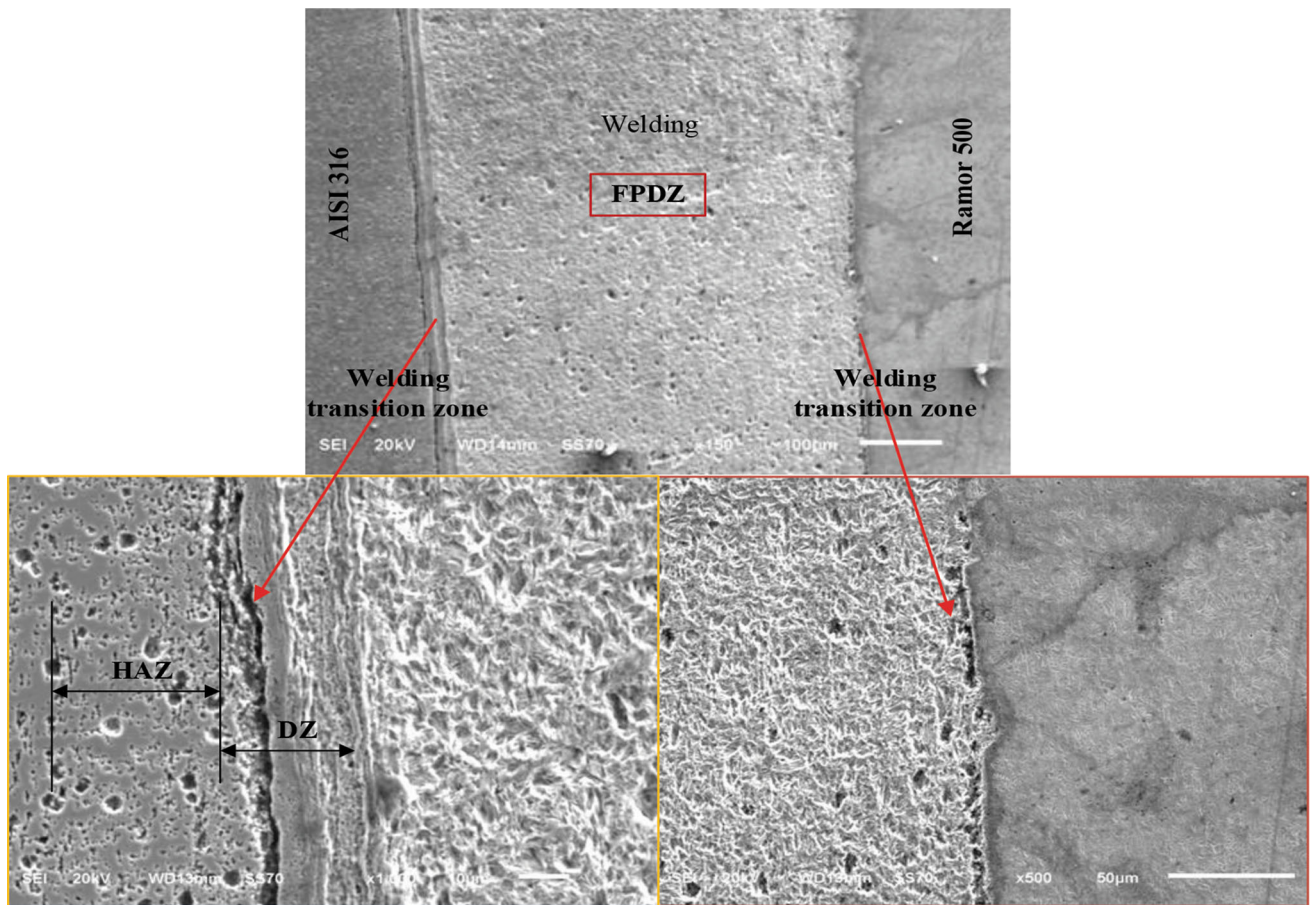


Fig. 5 SEM image of the weld cross section of sample S6

properties of these steels at all, due to the short processing time and low heat input.

Figure 6 shows EDS images of samples S1 and S6. As can be clearly noticed from the figure, the rates of Cr, Ni, and Mn increased but the rate of Fe decreased toward Ramor 500 steel from AISI 316 side in the sample S1. However, it was observed that the C rate did not change much. The sample S6 did not change too much. EDS analysis and concentration profiles were performed across the cross section of friction welded sample S6 at three different sites as shown in Fig. 7(a). When the EDS concentration profiles are examined (see in Fig. 7b), Cr and Ni diffuse to a high degree at a distance of about 50 μm from the armor steel, but Fe, on the other hand, shows a similar movement in the opposite direction. When compared to high density elements, the frictional heat generated at the interface would be high for low-density elements such as Mn, which has a low degree of diffusion due to their high boundary friction coefficients and low thermal conductivity (Ref 59-61). Moreover, the XRD patterns (Fig. 7c and d) showed that the Fe₅C₂, Cr₂₃C₆, and Cr₇C₃ phases were present in the joint region.

These intermetallic compounds were affirmed the presence of forging hardening and strengthening precipitates. The alloying elements Fe, Ni, Cr and Mn were confirmed from the EDS graph taken from the middle region of the joining line. (Fig. 7c).

Figure 8 shows the microhardness measurement results of friction welded joints made at 1 mm intervals along a linear line from the joint center to the base metal using two rotation speeds, 50 MPa friction pressure, and three different (3, 5, and 7 s) friction times. The distribution of microhardness differed in the weld zone and the adjoining zone. When the hardness profiles of the samples were analyzed, it is discovered that the maximum hardness in the Ramor 500 region was 608 Hv and then declined toward AISI 316 steel from the intermediary zone. Consequently, the hardness profiles changed based on the width of the heat-affected zones (HAZ). Previous studies have reported that the highest hardness values occurred in heat-affected zones, which adjacent to the friction joint line (Ref 51, 52, 62).

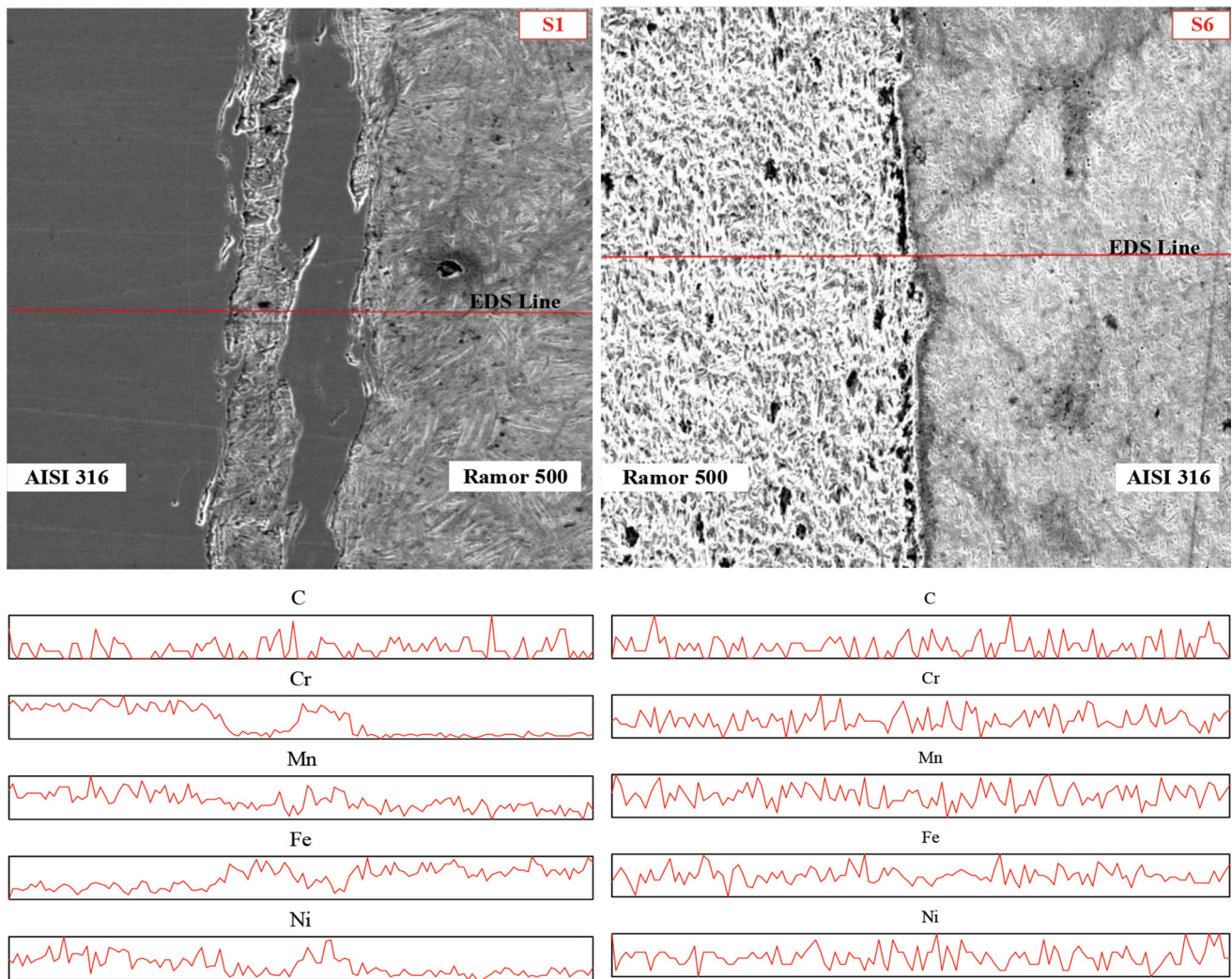


Fig. 6 Linear EDS analyses of S1 and S6 samples

3.2 Tensile Results of Welding Samples

Figure 9 presents the ultimate stress and % strain graphs of Ramor 500/AISI 316 steel pairs that were joined by friction welding at different welding parameters after tensile tests.

After determining the impact of welding parameters on microstructure images and hardness values, the tensile stresses, which are critical for welded joints, were determined. Tensile tests were performed for Ramor 500/AISI 316 steel pairs that were joined by friction welding. The tensile tests (Fig. 9) indicated that the selected parameters had a significant impact. The joints welded at 2200 rpm and 3 s (S1) parameters ultimate stress of 585.6 MPa. The lowest ultimate stress value was obtained as 441.5 MPa in the joints welded at 1800 rpm and 7 s (S6) parameters. When the structures in the welding transition zones of the samples S1 and S6 were examined, it is possible to say that this is an expected result. The macro-images after the tensile tests in Fig. 3 were analyzed. The sample S1 was waisted and had a ductile rupture on the AISI 316 side.

When the macrostructure of the sample S6 was examined, it was observed that the S6 sample had a ductile–brittle fracture between the HAZ and the weld metal. When the parameter impact was examined in general, it was observed that the ultimate strength of the joints decreased as the friction time prolonged at 1800 and 2200 rpm. However, when the rotation speed was increased from 1800–2200 rpm, the ultimate strength of the samples increased. Kırık et al. (Ref 63) stated that the tensile test results of AISI 1040 and AISI 304L materials, which they joined by friction welding, increased along with the increase in rotational speeds, which is increased in ultimate stresses. Maximum and minimum ultimate stress, yield strength and % strain of all samples are given in Table 4.

SEM images were taken for examine the structures forming on the fracture surfaces of the sample S6 after the tensile test. Figure 10 shows SEM images of the sample S6 at different magnitudes.

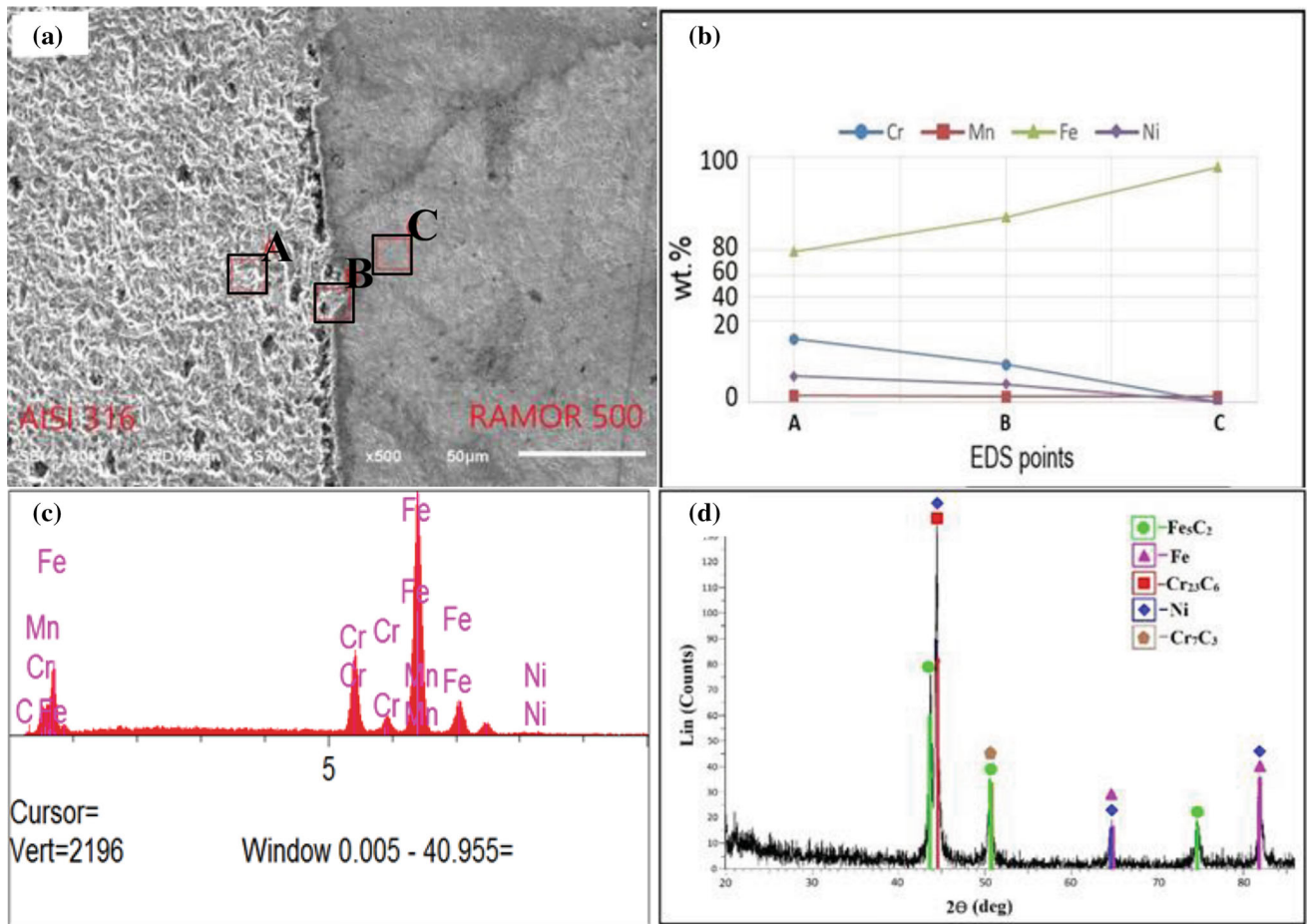


Fig. 7 EDS regions (a), Concentration profiles of S6 at different region (b), EDS graph of the whole region and (c) XRD pattern of S6 (d)

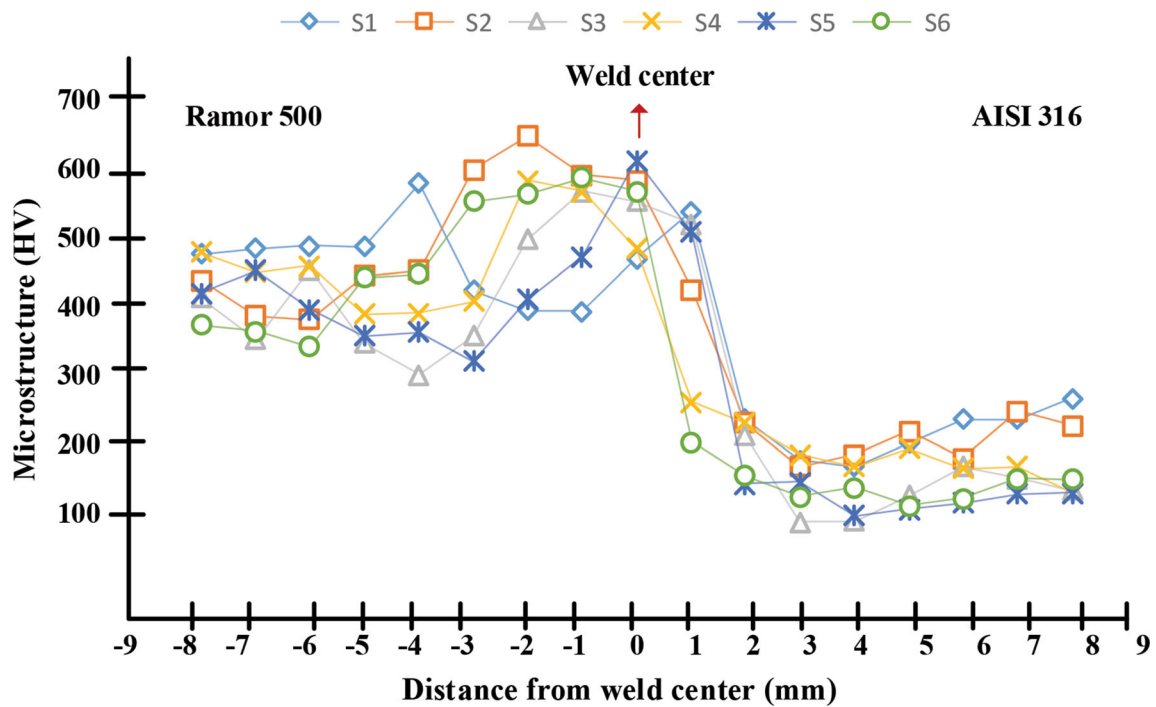


Fig. 8 Microhardness values of friction welded Ramor 500/AISI 316 joints

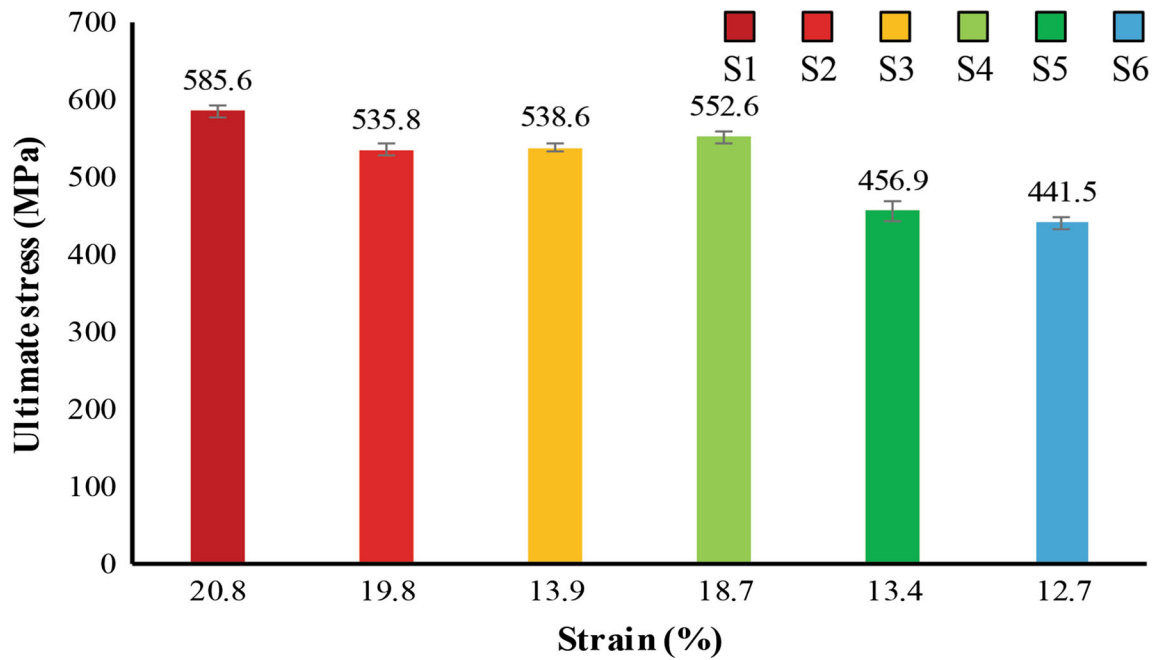


Fig. 9 Ultimate tensile strength (UTS) and strain (%) of samples welded

Table 4 Ultimate stresses, yield stresses and strain (%) values of specimens joined by friction welding

Specimen	Ultimate stress, MPa	Yield Stress, MPa	Strain, %
S1	578-595	483.6-503	19.6-21.8
S2	525-543.4	436.6-460	18.4-20
S3	531-544	429-461	11-15
S4	542-558	426-445.8	16-20.7
S5	441-471.7	334.6-370	12-14
S6	431-448.5	337.4-356.8	10.8-13

When examining the macrostructures of the fractures after the tensile tests (Fig. 3), it was observed that all the samples took place on the AISI 316 side. Post-tensile test SEM images of the sample S6 in Fig. 10 revealed the presence of microstructures with a fine-grained structure (Fig. 10b-c). Furthermore, when the structure in Fig. 10(a) was examined, it was observed that the sample displayed ductile deformation under load, but abrupt brittle fracture occurred after a certain deformation. Therefore, it can be asserted that mixed type fracture occurred in the sample S6.

4. Conclusions

In this study, Ramor 500 steel, which is used extensively in military applications, and AISI 316 steel, which is preferred especially in places exposed to corrosion due to its high chromium content, were joined by the friction welding method.

Welding was carried out at 1800 and 2200 rpm rotational speeds and 3, 5 and 7 s friction time parameters. Microstructural analyses and mechanical tests were carried out to determine the effects of the preferred parameters in the welding process on the weld joints. Obtained results are given below in order.

1. In the microstructure analyses of the welding parameters on the joints of Ramor 500/AISI316 steel pairs, it was clearly seen that parts that did not join and missing joints in the welding transition regions of the joint made with 1800 rpm and 7 s parameters (S6 sample). It has been observed that a good smooth joining occurs in the welding transition regions in the joints made at 2200 rpm and 3 s parameters.
2. In the linear EDS analyses performed perpendicular to the weld section, it was determined that there was a high level of chromium element on the AISI 316 side, and a high amount of Fe in the Ramor 500 steel. In the weld metal (FPDZ), AISI 316 steel melted at lower temperatures than Ramor 500 steel, so the chromium ratio was higher.
3. In the hardness examinations, the hardness values of Ramor 500 steel reached the maximum values in the HAZ region. On the AISI 316 steel side, the hardness of the base metal was lower than the weld metal and the hardness in the HAZ region.
4. In the tensile tests, the highest and lowest ultimate stresses are 585.6 MPa in sample S1 and 441.5 MPa in sample S6, respectively. Moreover, all samples were broken at the AISI 316 side after the tensile test.

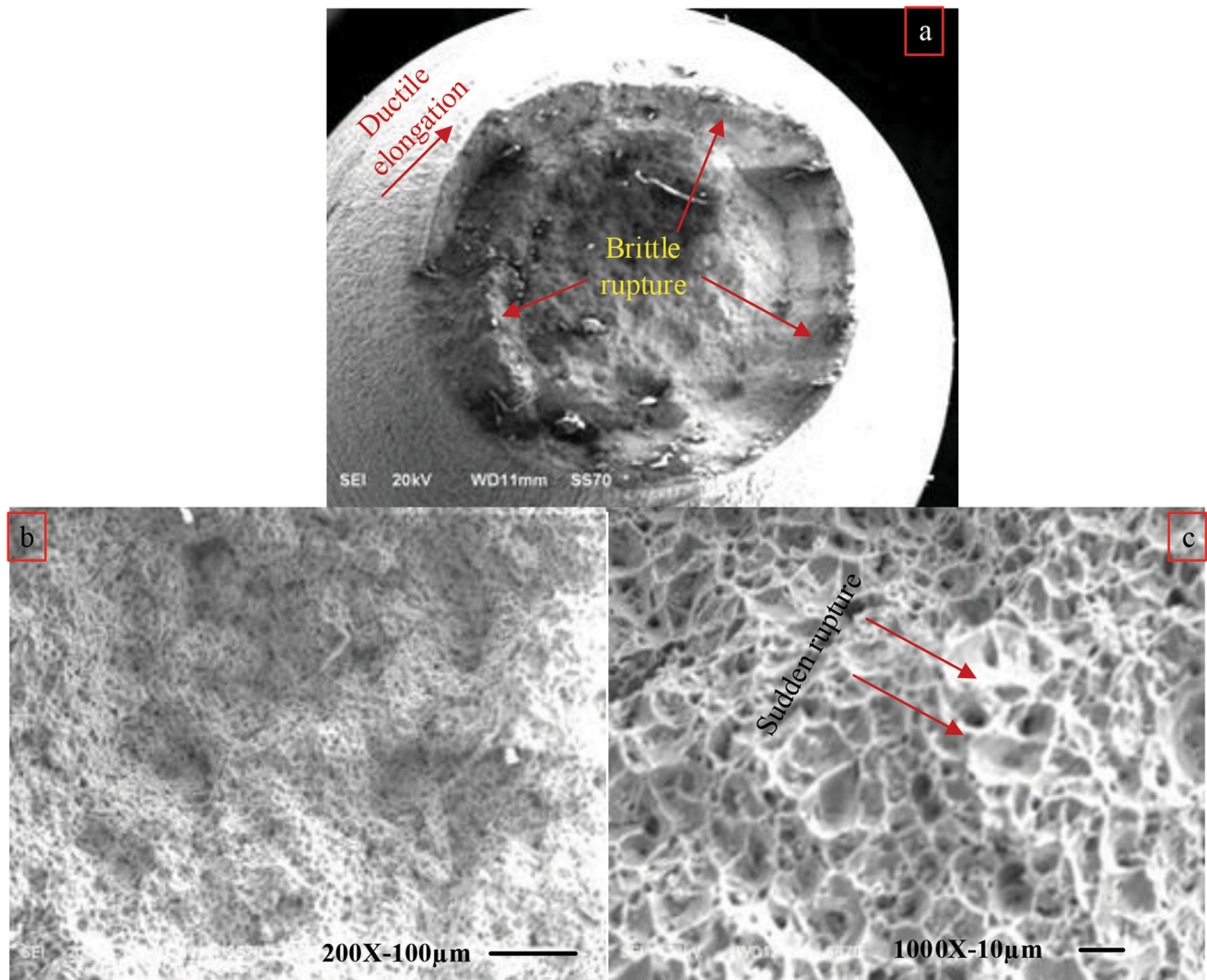


Fig. 10 Different sized fracture surfaces of the sample S6

- In the fracture analysis of the ruptured surfaces of the S6 sample after the tensile test, the rupture was realized as a ductile–brittle rupture mechanism (mix type).

Acknowledgments

The manuscript was not supported by any organization

Conflict of interest

The authors declare that they have no conflict of interest.

References

- M.C. Jo, S. Kim, D.W. Suh, S.S. Hong, H.K. Kim, S.S. Sohn, and S. Lee, Effect of Tempering Conditions on Adiabatic Shear Banding during Dynamic Compression and Ballistic Impact Tests of Ultra-High-Strength Armor Steel, *Mater. Sci. Eng. A*, 2020, **792**, p 139818.
- I. Barényi, O. Hireš, and P. Lipták, Changes in Mechanical Properties of Armoured UHSLA Steel ARMOX 500T after Over Tempering, *Probl. Mechatroniki Uzbroj Lot. inzynieria Bezpiecze nstwa Aviat Saf. Eng.*, 2013, **4**, p 7–13.
- A. Saxena, A. Kumaraswamy, G.M. Reddy, and V. Madhu, Influence of Welding Consumables on Tensile and Impact Properties of Multi-Pass SMAWArmoX 500T Steel Joints Vis-A-Vis Base Metal, *Def. Technol.*, 2018, **14**, p 188–195.
- L. Kuzmikova, *An Investigation of the Weldability of High Hardness Armor Steel*, Australia Pages, Wollongong, 2013, p 17–234
- A. Saxena, A. Kumaraswamy, S. Sethi, G.M. Reddy, and V. Madhu, Microstructural Characterization and High Strain Rate Plastic Flow Behavior of SMAWArmoX 500T Steel Joints from Spherical Indentation Experiments, *J. Mater. Eng. Perform.*, 2018, **27**, p 4261–4269.
- A. Saxena, A. Kumaraswamy, G.M. Reddy, and V. Madhu, Study of Tribological Characteristics of Multi-Pass SMAWArmoX 500T Steel Joints, *J. Mater. Eng. Perform.*, 2018, **27**, p 4300–4307.
- A. Saxena, A. Kumaraswamy, and V. Madhu, Investigation of S-D Effect on Plastic Flow Behavior of ArmoX 500T Steel, *J. Braz. Soc. Mech. Sci. Eng.*, 2018, **40**, p 463–477.
- J. Andersson, Welding Metallurgy and Weldability of Superalloys, *Metals (Basel)*, 2020, **10**(1), p 376. <https://doi.org/10.3390/met10010143>
- H. Dong, P.Y. Qi, X.Y. Li, and R.J. Llewellyn, Improving the Erosion-Corrosion Resistance of AISI 316 Austenitic Stainless Steel by Low-Temperature Plasma Surface Alloying with N and C, *Mater. Sci. Eng. A*, 2006, **431**(1–2), p 137–145. <https://doi.org/10.1016/j.msea.2006.05.122>
- J.R. Davis, *ASM Specialty Handbook*, ASM International, The Netherlands, 1997

11. M.F. McGuire, Austenitic stainless steels, *Stainless Steels for Design Engineers*. ASM International, The Netherlands, 2019
12. J.C. Lippold, *Welding Metallurgy and Weldability of Stainless Steels*, Wiley, Michigan, 2005
13. J.C. Lippold, *Duplex Stainless Steels*, Wiley, Ohio, 2005
14. K.H. Lo, C.H. Shek, and J.K.L. Lai, Recent Developments in Stainless Steels, *Mater. Sci. Eng. R*, 2009, **65**, p 39–104.
15. T. Saeid, A.A. Zadeh, and H. Assadi, Effect of Friction Stir Welding Speed on the Microstructure and Mechanical Properties of a Duplex Stainless Steel, *Mater. Sci. Eng. R*, 2008, **496**, p 262–268.
16. Y.S. Sato, T.W. Nelson, C.J. Sterling, R.J. Steel, and C.O. Pettersson, Microstructure and Mechanical Properties of Friction Stir Welded SAF 2507 Super Duplex Stainless Steel, *Mater. Sci. Eng. R*, 2005, **397**, p 376–384.
17. A. Urena, Weldability of a 2205 Duplex Stainless Steel using Plasma Arc Welding, *J. Mater. Process. Technol.*, 2007, **182**, p 624–631.
18. J. Nowacki and A. Lukojc, Structure and Properties of the Heat-Affected Zone of Duplex Steels Welded Joints, *J. Mater. Process. Technol.*, 2005, **164**, p 1074–1081.
19. N. Çavuşoğlu, Effect of Friction Welding Parameters on the Mechanical and Microstructural Properties of Dissimilar IN713C-AISI 4140 Joints, *J. Mater. Eng. Perform.*, 2022 <https://doi.org/10.1007/s11665-021-06474-w>
20. E. Cetkin, Y.H. Çelik, and S. Temiz, Microstructure and Mechanical Properties of AA7075/AA5182 Jointed by FSW, *J. Mater. Process. Technol.*, 2019, **268**, p 107–116. <https://doi.org/10.1016/j.jmatprotec.2019.01.005>
21. A. Heidarzadeh, S. Mironov, R. Kaibyshev, and G. Çam et al., Friction Stir Welding/Processing of Metals and Alloys: A Comprehensive Review on Microstructural Evolution, *Prog. Mater. Sci.*, 2021, **117**, p 100752.
22. S. Bahl, S. Suwas, and K. Chatterjee, Comprehensive Review on Alloy Design, Processing, and Performance of β Titanium Alloys as Biomedical Materials, *Int. Mater. Rev.*, 2021, **66**, p 114–139.
23. Z.H. He, J.S. Liu, D.W. Zhou, and T.A. Tao, Effect of Al-Foil Addition on Microstructure and Temperature Field of Laser Fusion Welded Joints of DP590 Dual-phase Steel and AZ31B Magnesium Alloy, *Trans. Nonferrous Metal Soc. China*, 2020, **30**, p 2669–2680.
24. H.T. My Nu, L.P. Minh, and N.H. Loc, A Study on Rotary Friction Welding of Titanium Alloy (Ti6Al4V), *Adv. Mater. Sci. Eng.*, 2019 <https://doi.org/10.1155/2019/4728213>
25. V.P. Singh, S.K. Patel, and B. Kuriachen, Mechanical and Microstructural Properties Evolutions of Various Alloys Welded through Cooling Assisted Friction-Stir Welding: A Review, *Intermetallics*, 2021, **133**, p 107122.
26. A.S. Pelliccione, R. SantAnna, M.H. Siqueira, A.F. Ribeiro, J.E. Ramos, O.P. Silva, and M.F. Pimentel, Failure Analysis of a Titanium Plate Heat Exchanger–Mechanical Fatigue, *Eng. Fail. Anal.*, 2019, **105**, p 1172–1188.
27. B. Keshtegar and M.E. Seghier, Modified Response Surface Method Basis Harmony Search to Predict the Burst Pressure of Corroded Pipelines, *Eng. Fail. Anal.*, 2018, **89**, p 177–199.
28. G. Zhi, X. Li, W. Bi, J. Tang, and Y. Rong, The Measurement and Analysis of Micro Bonding Force for Electroplated CBN Grinding Wheels Based on Response Surface Methodology, *Eng. Fail. Anal.*, 2015, **57**, p 377–388.
29. Y. Gong, F.Q. Ma, Y. Xue, C.S. Jiao, and Z.G. Yang, Failure Analysis on Leaked Titanium Tubes of Seawater Heat Exchangers in Recirculating Cooling Water System of Coastal Nuclear Power Plant, *Eng. Fail. Anal.*, 2019, **101**, p 172–179.
30. A. Tjernberg, Fatigue Life of a Friction Welded Joint with a Circular Crack in the Centre, *Eng. Fail. Anal.*, 2000, **7**, p 221–227.
31. L. Huang, K. Wang, W. Wang, J. Yuan, K. Qiao, T. Yang, P. Peng, and T. Li, Effects of Grain Size and Texture on Stress Corrosion Cracking of Friction Stir Processed AZ80 Magnesium Alloy, *Eng. Fail. Anal.*, 2018, **92**, p 392–404.
32. S. Bocchi, M. Cabrini, G. D'Urso, C. Giardini, S. Lorenzi, and T. Pastore, Stress Enhanced Intergranular Corrosion of Friction Stir Welded AA2024-T3, *Eng. Fail. Anal.*, 2020, **111**, p 104483.
33. R. Rajasekaran, A.K. Lakshminarayanan, R. Damodaram, and V. Balasubramanian, Stress Corrosion Cracking Failure of Friction Stir Welded Nuclear Grade Austenitic Stainless Steel, *Eng. Fail. Anal.*, 2021, **120**, p 105012.
34. H. Jian, Y. Wang, X. Yang, and K. Xiao, Microstructure and Fatigue Crack Growth Behavior in Welding Joint of Al-Mg Alloy, *Eng. Fail. Anal.*, 2021, **120**, p 105034.
35. L.L. Huetsch, K. Herzberg, J.F. dos Santos, and N. Huber, A Study on Local Thermal and Strain Phenomena of High-Speed Friction Stir-Processed Mg AZ31, *Weld. World*, 2013, **57**, p 515–521.
36. Y. Guo, X. Zhang, X. Qian, and J. Li, Study on Residual Stress Distribution of 2024-T3 and 7075-T6 Aluminum Dissimilar Friction Stir Welded Joints, *Eng. Fail. Anal.*, 2020, **118**, p 104911.
37. S. Aliasghari, A. Rogov, P. Skeldon, X. Zhou, A. Yerokhin, A. Aliabadi, and M. Ghorbani, Plasma Electrolytic Oxidation and Corrosion Protection of Friction Stir Welded AZ31B Magnesium Alloy-Titanium Joints, *Surf. Coat. Technol.*, 2020, **393**, p 125838.
38. J.W. Choi, H. Liu, K. Ushioda, and H. Fujii, Dissimilar Friction Stir Welding of Immiscible Titanium and Magnesium, *Materialia*, 2019, **7**, p 100389.
39. K. Singh, G. Singh, and H. Singh, Microstructure and Mechanical Behaviour of Friction-Stir-Welded Magnesium Alloys: As-Welded and Post Weld Heat Treated, *Mater. Today Commun.*, 2019, **20**, p 100600.
40. W. Li, P.L. Niu, S.R. Yan, V. Patel, and Q. Wen, Improving microstructural and tensile properties of AZ31B magnesium alloy joints by stationary shoulder friction stir welding, *J. Manuf. Process.*, 2019, **37**, p 159–167.
41. J. Unfried, C.M. Garzon, and J.E. Giraldo, Numerical and Experimental Analysis of Microstructure Evolution During Arc Welding in Armor Plate Steels, *J. Mater. Process. Technol.*, 2009, **209**, p 1688–1700. <https://doi.org/10.1016/j.jmatprotec.2008.04.025>
42. F. Sarsilmaz, I. Kirik, and S. Bati, Microstructure and Mechanical Properties of armor 500/AISI2205steel Joint by Friction Welding, *J. Manuf. Process.*, 2017, **28**, p 131–136. <https://doi.org/10.1016/j.jma.2017.05.025>
43. S. Taskaya, A. Kaya Gur, and A. Orhan, Joining of Ramor 500 Steel by Submerged Welding and its Examination of Thermal Analysis in ANSYS Package Program, *Therm. Sci. Eng. Prog.*, 2019, **11**, p 84–110. <https://doi.org/10.1016/j.tsep.2019.02.002>
44. N. Ezgi İpek and F. Elaldi, Analysis of Welding Groove Angle and Geometry on Strength of Armor Steel, *Mater. Manuf. Process.*, 2012, **27**(12), p 1437–1441. <https://doi.org/10.1080/10426914.2012.709343>
45. B. Savic and A. Cabrilo, Effect of Heat Input on the Ballistic Performance of Armor Steel Weldments, *Materials*, 2021, **14**, p 3617. <https://doi.org/10.3390/ma14133617>
46. G. Magudeeswaran, V. Balasubramanian, and G. Madhusudan Reddy, Metallurgical Characteristics of Armour Steel Welded Joints used for Combat Vehicle Construction, *Def. Technol.*, 2018, **14**, p 590–606. <https://doi.org/10.1016/j.dt.2018.07.021>
47. M.P. Prabakaran and G.R. Kannan, Optimization of Laser Welding Process Parameters in Dissimilar Joint of Stainless Steel AISI316/ AISI1018 Low Carbon Steel to Attain the Maximum level of Mechanical Properties through PWHT, *Opt. Laser Technol.*, 2019, **112**, p 314–322. <https://doi.org/10.1016/j.optlastec.2018.11.035>
48. S.A. Seregin and V.P. Sabatsev, Friction Welding of Plastically Deformed Steel, *WeldProd*, 1975, **22**, p 34–35.
49. I. Kirik, N. Ozdemir, and U. Caligulu, Effect of Particle Size and Volume Fraction of the Reinforcement on the Microstructure and Mechanical Properties of Friction Welded MMC to AA 6061 Aluminum Alloy, *Kovove Mater.*, 2013, **51**, p 221–227. https://doi.org/10.4149/km_2013_4_221
50. M. Sahin, Joining of Stainless-Steel and Aluminium Materials by Friction Welding, *Int. J. Adv. Manuf. Technol.*, 2009, **41**, p 487–497. <https://doi.org/10.1007/s00170-008-1492-7>
51. K. Karthick, S. Malarvizhi, and V. Balasubramanian, Mechanical Properties and Microstructural Characteristics of Rotary Friction Welded Dissimilar Joints of Rolled Homogeneous Armor Steel and Medium Carbon Steel, *J. Mech. Behav. Mater.*, 2021, **30**(1), p 171–178. <https://doi.org/10.1515/jmbm-2021-0017>
52. P. Sathiyaa, S. Aravindan, and A. Noorul Haq, Some Experimental Investigations on Friction Welded Stainless Steel Joints, *Mater. Des.*, 2008, **29**(6), p 1099–1109. <https://doi.org/10.1016/j.matdes.2007.06.006>
53. U. Caligulu, M. Yalcinoz, N. Kati, Z. Balalan, and S. Islak, The Effects of Rotation Speed and Friction Time for Joining of AISI 4340-2205 Steels by Friction Welding, *Metallofiz Noveishie Tekhnol.*, 2015, **37**(5), p 665–681.

54. U. Caligulu, M. Yalcinoz, M. Turkmen, and S. Mercan, x-ray Radiography of AISI 4340-2205 Steels Welded by Friction Welding, *Mater. Technol.*, 2016, **50**(1), p 39–45. <https://doi.org/10.17222/mit.2014.211>
55. A. Günen, S. Bayar, and M.S. Karakaş, Effect of Different Arc Welding Processes on the Metallurgical and Mechanical Properties of Ramor 500 Armor Steel, *ASME, J. Eng. Mater. Technol.*, 2020, **142**(2), p 021007. <https://doi.org/10.1115/1.4045569>
56. B. Skowrońska, J. Szulc, M. Bober, M. Baranowski, and T. Chmielewski, Selected Properties of RAMOR 500 Steel Welded Joints by Hybrid PTA-MAG, *J. Adv. Join. Process.*, 2022, **5**, p 100111. <https://doi.org/10.1016/j.jajp.2022.100111>
57. S. Naveen Kumar, V. Balasubramanian, S. Malarvizhi, A. Hafeezur Rahman, and V. Balaguru, Effect of Failure Modes on Ballistic Performance of Gas Metal Arc Welded Dissimilar Armour Steel Joints, *CIRP J. Manuf. Sci. Technol.*, 2022, **37**, p 570–583. <https://doi.org/10.1016/j.cirpj.2022.03.004>
58. C. Sharma, V. Upadhyay, D.K. Dwivedi, and P. Kumar, Mechanical Properties of Friction Stir Welded Armor Grade Al-Zn-Mg Alloy Joints, *Trans. Nonferrous Metal Soc. China*, 2017, **27**, p 493–506. [https://doi.org/10.1016/S1003-6326\(17\)60056-6](https://doi.org/10.1016/S1003-6326(17)60056-6)
59. J.S. Tiley, D.W. Mahaffey, T. Alam, T. Rojhirunsakool, O. Senkov, T. Parthasarthy, and R. Banerjee, Strengthening Mechanisms in an Inertia Friction Welded Nickel-Base Superalloy, *Mater. Sci. Eng. A*, 2016, **662**, p 26–35. <https://doi.org/10.1016/j.msea.2016.03.030>
60. V.V. Sathyanarayana, R.G. Madhusudhan, and T. Mohandas, Dissimilar Metal Friction Welding of Austenitic-Ferritic Stainless Steels, *J. Mater. Process. Technol.*, 2005, **160**, p 128–137. <https://doi.org/10.1016/j.jmatprotec.2004.05.017>
61. D. Ananthapadmanaban, R.V. Seshagiri, A.P. Nikhil, and K. Rao, A Study of Mechanical Properties of Friction Welded Mild Steel to Stainless Steel Joints, *Mater. Des.*, 2009, **3**, p 2642–2646. <https://doi.org/10.1016/j.matdes.2008.10.030>
62. N. Özdemir, Investigation of the Mechanical Properties of Friction-Welded Joints between AISI 304L and AISI 4340 Steel as a Function Rotational Speed, *Mater. Lett.*, 2005, **59**, p 2504–2509. <https://doi.org/10.1016/j.matlet.2005.03.034>
63. I. Kirik, N. Ozdemir, E.H. Firat, and U. Caligulu, Optimization of Tensile Strength of Friction Welded AISI 1040 and AISI 304L Steels According to Statistics Analysis (ANOVA), *Mater. Test.*, 2013, **55**(6), p 435–441. <https://doi.org/10.3139/120.110455>

Publisher's Note Springer Nature remains neutral with regard to jurisdictional claims in published maps and institutional affiliations.

Springer Nature or its licensor (e.g. a society or other partner) holds exclusive rights to this article under a publishing agreement with the author(s) or other rightsholder(s); author self-archiving of the accepted manuscript version of this article is solely governed by the terms of such publishing agreement and applicable law.